Journal of Vacuum Science and Technology B

RESEARCH ARTICLE | OCTOBER 17 2023

Investigation of polymer template removal techniques in three-dimensional thin-shell nanolattices FREE

Special Collection: Papers from the 66th International Conference on Electron, Ion and Photon Beam Technology and Nanofabrication (EIPBN 2023)

Vijay Anirudh Premnath ; Chih-Hao Chang

J. Vac. Sci. Technol. B 41, 062805 (2023)
https://doi.org/10.1116/6.0003036

JVST B
Journal of Vacuum Science & Technology B

ARTICLE

pubs.aip.org/avs/jvb

Investigation of polymer template removal techniques in three-dimensional thin-shell nanolattices

Cite as: J. Vac. Sci. Technol. B 41, 062805 (2023); doi: 10.1116/6.0003036
Submitted: 2 August 2023 · Accepted: 18 September 2023 ·
Published Online: 17 October 2023

Vijay Anirudh Premnath and Chih-Hao Chang[a)]

AFFILIATIONS

Walker Department of Mechanical Engineering, University of Texas at Austin, Austin, Texas 78712

Note: This paper is part of the Special Topic Collection: Papers from the 66th International Conference on Electron, Ion and Photon Beam Technology and Nanofabrication (EIPBN 2023).

[a)]**Email:** chichang@utexas.edu

ABSTRACT

Recent advanced in nanofabrication has enabled various opportunities for research and development in photonic crystals, integrated circuits, and nanostructured materials. One interesting class of emerging materials is nanolattices, which consist of hollow-core, thin-shell elements fabricated using thin-film deposition on three-dimensional polymer templates. While many applications of nanolattices have been demonstrated, the residual polymer in the nanolattice can be problematic and is not well understood. This research investigates the effectiveness of different template removal techniques, including oxygen plasma etching, solvent dissolution, and thermal desorption. The rates and effectiveness of resist removal for the different techniques are quantified using spectroscopic ellipsometry, which enables precise measurement of the effective refractive index and calculation of the residual polymer. A three-phase Maxwell–Garnett effective medium model is used to calculate the residual polymer in the nanolattices. This work demonstrates that the temperature treatment is most effective at template removal, which can be used to improve the fabrication of nanolattices for mechanical, optical, and thermal applications.

I. INTRODUCTION

Nanofabrication technology has opened enormous opportunities in several fields such as semiconductor fabrication, optical engineering, and energy storage. Nanolattices are utilized in the creation of lightweight materials with extraordinary mechanical properties, such as high stiffness-to-weight ratio, deformability, and recovery rates.[1–4] They can also be used in the design of advanced energy storage systems such as batteries and supercapacitors due to their large surface areas to volume ratio, facilitating higher energy densities and faster charging times.[2] Furthermore, their low thermal conductivity allows these structures to act as excellent thermal insulators, making them suitable for various applications in electronics and space technology.[5] Nanolattices are also highly porous and can have a refractive index as low as 1.025,[6] which can be used as a low-index film for optical applications. Additionally, nanolattices can also be utilized to manipulate light on the nanoscale, providing applications in photonic devices, solar cells, and light-emitting diodes (LEDs).[7,8]

There are several methods to fabricate nanolattices including two-photon polymerization (TPP),[9–13] which is a high-resolution, direct-write technique capable of creating complex 3D nanostructures. Other top-down techniques include electron beam lithography, which can be used to focus a beam of electrons to induce the deposition of inorganic materials to fabricate complex 3D structures.[14,15] In addition, interference lithography[16,17] is a parallel technique that employs two or more interfering waves to form desired patterns on a photosensitive resist. In addition to top-down lithography approaches, self-assembly techniques enable nanoscale elements to be chemically designed to self-assemble into organized 3D geometry.[18,19] Another way to create a mask to pattern 3D nanostructures is to use a near-field phase mask[20] or colloidal self-assembly of nanoparticles.[21,22] This technique leverages the Talbot effect, a wave propagation phenomenon wherein a periodic optical field can reproduce itself at specific distances, known as Talbot lengths.[23] By manipulating this effect, complex three-dimensional intensity patterns can be

generated to expose underlying photoresist, extending beyond conventional planar patterning. This process substantially enhances nanoscale manufacturing capabilities, finding applications in photonics and metamaterials.

Once the nanolattice geometry is defined by lithography in the polymer resist, a conformal coating can be applied using atomic layer deposition (ALD).[3,4,11,21,22,24] ALD utilizes sequential gas phase chemical processes by splitting the film growth into two self-limiting half reactions,[25] allowing the film to be deposited one atomic layer per cycle. This leads to precise and conformal thin films with atomic-level control over thickness and composition. This method is particularly useful in nanolattice fabrication as it can accurately deposit materials on the complex 3D structures of nanolattice.[24] After ALD deposition, the polymer template can be removed through plasma etching[3,11] or thermal desorption[4,26] to result in a free-standing nanolattice structure. However, the effectiveness of these polymer removal processes has not been quantitatively studied. This is critical, as any residual polymer can potentially affect the physical properties of the resultant nanolattices.

In this work, we examine the effectiveness of template removal processes and their effects on the optical properties of the fabricated nanolattices. Three different techniques of polymer removal have been extensively studied, namely, thermal desorption using a furnace, solvent dissolution using n-methyl-2-pyrrolidone (NMP), and oxygen plasma etching (O_2 PE). The 3D nanolattice samples studied are fabricated using colloidal phase lithography and have been subjected to the three template removal processes with different process times. To quantify the polymer removal rate and effectiveness of each process, the effective refractive index of the nanolattice film is measured using spectroscopic ellipsometry (SE). An optical thin-film model using a three-phase Maxwell–Garnett (MG) effective medium model is developed to calculate the volume fraction of residual polymer. This work furthers the understanding of the template removal process in the fabrication of nanolattices and can find applications in nanoarchitected materials, thermal insulation coating, and nanophotonics.

II. EXPERIMENTAL METHODOLOGY

The fabrication process of the 3D nanolattice structures used in the polymer removal experiments is multifaceted and implemented in a series of steps as explained in detail in previous research.[6,26] The schematic of the overall fabrication process and the three template removal steps are depicted in Fig. 1. The process starts with silicon substrates (100 mm, University Wafer), which is coated with 100 nm of antireflection coating (i-con-16, Brewer Science) and 300 nm thickness of positive-tone photoresist (PFi-88A2, Sumitomo Chemical). The antireflective coating (ARC) prevents back reflections from the wafer and minimizes the formation of standing waves and increases the adhesion between the resist layer and the substrate. Polystyrene spheres with diameters of 500 nm (2.5% aqueous solution, Polysciences) are assembled to form a hexagonal close-packed array on the photoresist. The samples are illuminated with a UV laser with a wavelength of 325 nm with a nominal dose of 90 mJ/cm^2, which results in a 3D intensity pattern due to light diffraction and interference effects, as shown in Fig. 1(a). Postlithography, the nanospheres are removed using an ultrasonication bath, and the photoresist is developed CD-26 (CD-26, Microposit) and rinsed in de-ionized water. This process results in a resist template consisting of polymer 3D nanolattices.

The polymer template samples are then subjected to 225 cycles of Al_2O_3 ALD (Cambridge Savannah TM 200), which

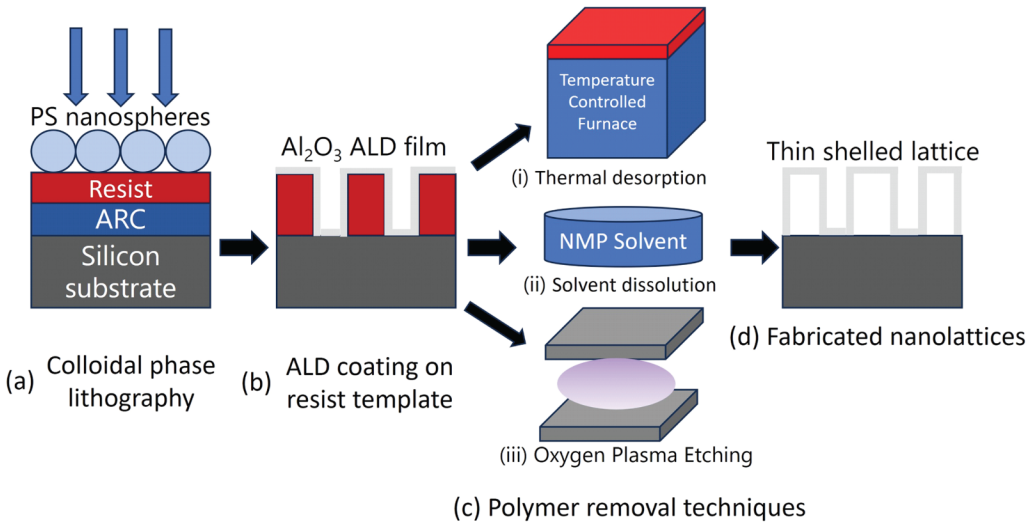

FIG. 1. Schematic of the nanolattice fabrication process involving (a) deposition of ARC, PR, and nanospheres with 500 nm diameter followed by lithography and development. (b) Samples are subjected to ALD over the template. (c) Three types of resist removal techniques include (i) thermal desorption, (ii) solvent dissolution, and (iii) oxygen plasma etching. (d) Final thin-shell lattice after polymer is removed.

approximates to about 24.75 nm thickness. The formation of Al_2O_3 is a combination of two half reactions between trimethyl aluminum (TMA) and de-ionized water. The deposition pressure is maintained at 550 mTorr, with the chamber bed temperature of 90 °C. Al_2O_3 conformally coats over the 3D volumetric intensity patterns generated from lithography, as illustrated in Fig. 1(b).

The samples are then subjected to three different types of resist removal processes, as illustrated in Fig. 1(c). In the thermal desorption process (i), the samples are placed in a temperature-controlled furnace and heated to 550°C with a ramp rate of 1 °C/min. The temperature is maintained for 4 h before cooling down to room temperature at the rate of 5 °C/min. This process removes all polymer template that is present in the structures, as illustrated in Fig. 1(d). The second template removal process is solvent dissolution (ii), where the polymer samples with ALD coating are immersed in the NMP solvent, a common positive photoresist remover. The samples are then rinsed in DI water and dried. The third template removal process is O_2 PE (iii), where the samples are etched in a parallel plate plasma etcher (part, company). In this procedure, the samples undergo etching at 115 W RF power, 450 mTorr pressure, with an oxygen flow rate of 10 SCCM to eliminate all polymers. These settings are optimized to deliver the maximum plasma power in the briefest duration in the equipment limits.

Thermal desorption involves heating the material beyond the melting, causing the photoresist polymers to combust and evaporate from the material's surface. The thermal treatment process can be monitored using differential scanning calorimetry, which indicates that the polymer starts combusting at 300 °C and stops at around 500 °C to show that there are no polymers left.[27] The temperature process is performed over a long duration to ensure that substrate heating is uniform. NMP is a common positive photoresist remover and dissolves resist. To dissolve the polymer template in the current work, the solution needs to penetrate through the nanoscale pores in the ALD layers, which is believed to be the rate-limiting step. Pockets of resist remains can be identified when the pore sizes are negligible for the NMP solution to infiltrate through. In contrast, oxygen plasma etching uses activated oxygen ions to react with the resist and turn it into volatile species that can be pumped away. While plasma can better penetrate through the ALD films and into the resist layers, the etch rate is considerably slower and limited by the reaction rate.

To quantify the effectiveness of resist removal by the three different methods, the effective refractive indices of the resultant nanolattice films are characterized using SE. SE is a nondestructive, broadband optical technique for probing the optical properties of thin films by measuring the change in the polarization state of light using two parameters including the amplitude ratio (Ψ) and phase difference (Δ) after reflection from or transmission through a sample.[28] The acquired data are fitted against theoretical models in a regression analysis, providing comprehensive information about the film's index and thickness. In our work, a wavelength range between 200 and 1600 nm is measured, and the nanolattice layer is modeled as an isotropic Cauchy layer that assumes that the refractive index is identical along all directions. The Cauchy layer is placed over a native oxide layer, which is iteratively fitted for thickness to obtain accurate representation of real samples, which might have a native oxide deposition over the bare silicon surface. For the samples obtained from the NMP and O_2 plasma etching removal process, an ARC layer is included below the nanolattice in the SE model.

III. RESULTS AND DISCUSSION

A. Fabrication challenges

An SEM image representing the fabricated lattices after subjecting them to thermal desorption is shown in Fig. 2. It is observed from the images that the resist removal using a temperature-controlled furnace is most effective since all polymer is removed from the sample. The drawback is that the process is time consuming, which in this case takes about 8 h and 50 min to reach the setpoint temperature of 550 °C. The slow ramp up rate is needed to ensure that the nanolattice does not collapse during the phase transformation, which is limited by the shell thickness. The temperature cycle also includes 4 h dwell time at the setpoint temperature of 550 °C to completely evaporate the resist material, followed by ramping down at a rate of 5 °C/min. The whole process takes over 14 h to complete.

To decrease the processing time, the second polymer removal technique examined is solvent dissolution where the samples are immersed in NMP for 0, 5, 10, and 15 min. After 15 min, the rate of polymer removal slows down because most of the polymer has already been removed. This result indicates that there are residual polymers trapped in confined spaces that are not easily accessible by the NMP solution. The SEM images of fabricated nanolattices after 5 and 10 min of NMP dissolution are shown in Fig. 3. When exposed to NMP dissolution, photoresist integrates into the solvent, creating a hydrated matrix that can be rinsed away to produce porous nanolattices. It can be observed that the dark grey regions on the images in Figs. 3(a) and 3(b) correspond to the residual resist present after 5 min of dissolution. Such residual resist is less observed after 10 min, as shown in Figs. 3(c) and 3(d). The faint grey captured by the SEM indicates that the resist is removed progressively over time. While NMP has a high photoresist dissolution rate, the need for the liquid to permeate the nanostructures can

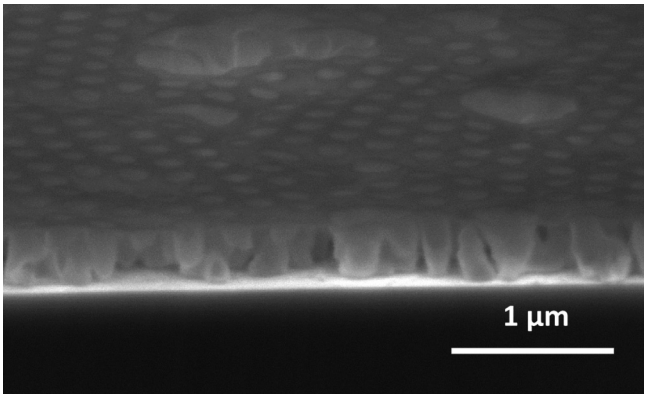

FIG. 2. Fabrication results of nanolattices after removing the polymer template in the furnace (thermal desorption). The SEM image of nanolattices fabricated with 500 nm diameter particles and 300 nm resist height.

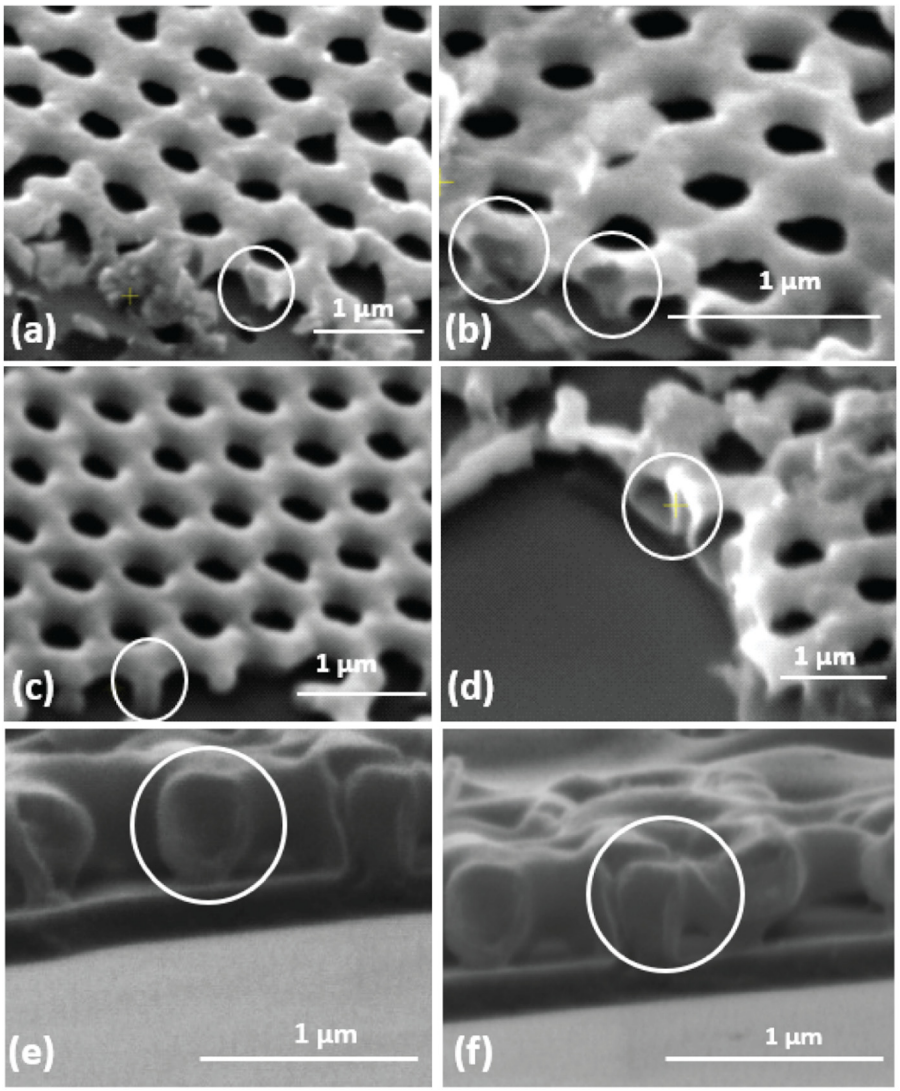

FIG. 3. Images of lattice post subjecting them to resist removal processes. (a) and (b) SEM images with prominent gray regions representing 5 min of NMP exposure, (c) and (d) images depict faint grey regions for resist removal in the nanolattices after 10 min of NMP dissolution, (e) SEM image with prominent gray regions representing 5 min of plasma etching, (f) SEM image depict milder gray regions for resist removal in the nanolattices after 10 min of the plasma etching process.

slow the template removal process. Though the SEM images can be used to qualitatively examine the presence of residual resist, the amount of resist remaining cannot easily be identified.

The third polymer template removal method is O_2 PE, also known as ashing, which uses a highly reactive environment of oxygen ions to remove the photoresist. During O_2 PE, photoresist fragments are removed, leaving an air-filled porous structure due to the preferential etching of the resist as shown in Fig. 4. Unlike NMP dissolution, O_2 PE is a dry etching process and can be more permeable within the 3D nanolattice structures. However, the etch rate is not as high as solvent dissolution, which might require longer etch times. Thus, it is noted from Figs. 3(e) and 3(f) that both images contain prominent dark grey regions, indicating the presence of resist after exposures to 5 and 10 min of the plasma etching process. This indicates that the volume fraction of residual resist even after 10 min is significant compared to the NMP dissolution.

B. Spectroscopic ellipsometry measurements

Once the templates have been removed, the residual polymer in the nanolattice samples can be quantitatively examined using SE. An illustrative measurement and fitted data with respect to wavelength for a nanolattice sample are depicted in Fig. 4. Here, the measured ratios of polarization amplitudes (Ψ) and phases (Δ) in reflected light are compared with an optical model to extract physical properties like thickness and refractive index for the thermal desorption sample. Iterative optimization reduces the mean square error (MSE) until the modeled film stack agrees with the experimentally measured values. Similar SE measurement and fitting

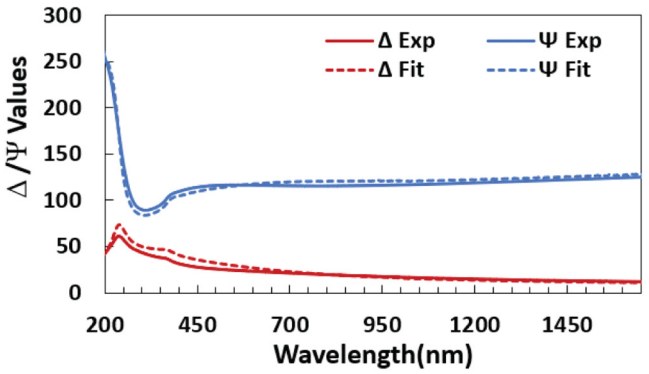

FIG. 4. Measured and fitted Δ/Ψ values over the wavelength spectrum for a nanolattice sample subjected to thermal desorption. The close agreement between the two indicates that the measured effective index is accurate.

results were obtained for the NMP and O_2 PE samples, albeit with slightly higher MSE. The MSE value for the nanolattice fabricated using the thermal desorption process is 23.1 and is significantly lower than when using NMP and O_2 PE, which are 54.8 and 42.4, respectively. The differences in converged MSE values signify that the corresponding index measurements can have higher deviations for NMP and O_2 PE etching process, which can be attributed to nonuniform polymer residual across the sample.

C. Investigation of the resist removal process

The refractive indices of the nanolattice films as measured using SE are plotted versus treatment time for the three-template removal process, as shown in Fig. 5(a). Here, the error bar is 2.3×10^{-4} as defined by the standard deviation of 10 separate measurements on the sample. The measured index for the thermal treatment process is 1.0661, which is much lower than the index of Al_2O_3 due to high porosity. Since there is a negligible amount of polymer residual in the temperature-treated nanolattice, this value is plotted as the reference data using dashed lines. The process takes over 14 h, therefore, the effectiveness at shorter time frames cannot be evaluated. The effective indices for the NMP and O_2 PE processes are also plotted after 0-, 5-, 10-, and 15-min treatment. It is noted that the measured indices for both follow similar trends. The index starts at 1.7017 prior to the template removal process, where the nanolattice consists of both Al_2O_3 ALD and photoresist. As the treatment time increases, the measured indices for NMP and O_2 PE decrease. It can be noted that the resist removal rate is slightly higher for NMP, since after 5 min the index reduces to 1.2364 as compared to about 1.4876 for O_2 PE. The difference in polymer removal can be attributed to the NMP solvent being a wet etch process with a higher dissolution rate. In addition, the NMP solution has low viscosity and can be wicked within the nanolattice to facilitate polymer dissolution. After 10 min the measured indices stabilize and the rates of removal slow, reaching 1.1784 for NMP and 1.2594 for the O_2 PE process. After 15 min, the measured indices for NMP and O_2 PE reach final values of 1.1336 and 1.1519, respectively. It is important to note that the measured

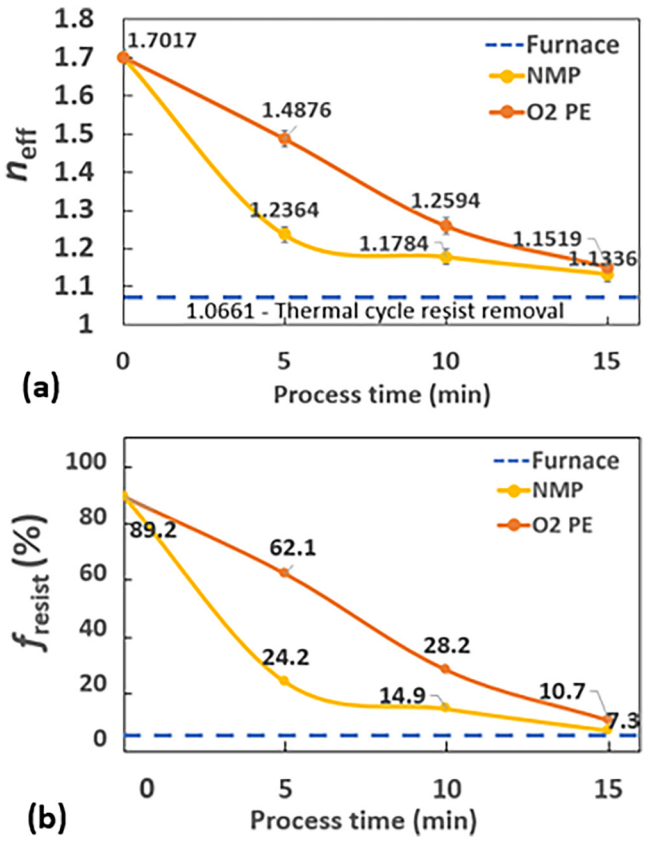

FIG. 5. (a) Measured effective refractive indices of the nanolattices vs process time. (b) Calculated volume fraction of residual polymer vs process time using the MG model.

indices for NMP and O_2 PE do not reach that of the temperature process, which indicates that some residual polymer remains for both processes.

Based on the effective medium theory, the measured indices can be used to calculate the volume fraction of the residual resist. In this model, the Al_2O_3 ALD and polymer can be considered inclusions in the host medium consisting of air.[29] We first consider the case for thermal desorption, where all polymers are removed, resulting in a two-phase system. The effective index and volume fraction can be calculated using the two-phase MG model[29]

$$\frac{n_{\text{eff}}^2 - n_{\text{air}}^2}{n_{\text{eff}}^2 + 2n_{\text{air}}^2} = f_{\text{ALD}} \left[\frac{n_{\text{ALD}}^2 - n_{\text{air}}^2}{n_{\text{ALD}}^2 + 2n_{\text{air}}^2} \right],$$

where n_{eff} is the effective refractive index observed from SE, n_{air} is the index of the host medium or air, and n_{ALD} and f_{ALD} are the refractive index and volume fraction of Al_2O_3 inclusions, respectively. For a given effective index of 1.0661 and using n_{ALD} of 1.77 at 632 nm, f_{ALD} is calculated as 10.4%. Note the calculated f_{ALD} can serve as a reference for the volume fraction of Al_2O_3 for all the

samples since the same photoresist template and ALD thickness are used. For the samples subjected to NMP dissolution and O_2 PE, the residual photoresist can be modeled as an additional inclusion along with Al_2O_3 in a host medium of air, resulting in a three-phase MG equation[29]

$$\frac{n_{\text{eff}}^2 - n_{\text{air}}^2}{n_{\text{eff}}^2 + 2n_{\text{air}}^2} = f_{\text{ALD}}\left[\frac{n_{\text{ALD}}^2 - n_{\text{air}}^2}{n_{\text{ALD}}^2 + 2n_{\text{air}}^2}\right] + f_{\text{resist}}\left[\frac{n_{\text{resist}}^2 - n_{\text{air}}^2}{n_{\text{resist}}^2 + 2n_{\text{air}}^2}\right],$$

where f_{resist} and n_{resist} are the volume fraction and refractive index of resist (1.6560 at 632 nm). Since the volume of Al_2O_3 remains the same irrespective of the resist removal process, f_{ALD} is set to a value of 10.4% based on the two-phase MG model.

The calculated f_{resist} values as functions of process time are shown in Fig. 5(b). The results indicate that about 89.2% of resist is present in the lattice at the beginning of the resist removal process at 0 min. When subjected to NMP dissolution, the volume fraction reduces to 24.2%, 14.9%, and 7.3% at 5, 10, and 15 min, respectively. Similarly, for O_2 PE, the volume fraction of resist reduces to 62.1%, 28.2%, and 10.7% of resist for 5, 10, and 15 min, respectively. It can be noted that the resist volume fraction reduces faster in NMP solvent dissolution compared to O_2 PE, confirming that the former has a higher template removal rate. It can be noted that the calculated total volume fractions of ALD and photoresist at 0 min are close to 100%, leaving close to no air pores. This result is not physical and can be attributed to the fact that the mixing formula of the MG equation is asymmetric, and the model fails when the volume fractions of inclusions and host are comparable.[29] At the longest etch times, the calculated f_{resist} are much lower at 10.7% and 7.3%, which is in the regime where the MG model is valid.

The experimental data demonstrate that it is possible to quantify the polymer residual in the nanolattices using SE. However, there are some challenges that can limit the accuracy of this approach. The first is the variations in the fabricated nanolattice geometry, which is caused by colloidal assembly defects, under or overexposure, and structure collapse. Such variations can result in nonuniform structures and increase error in the SE fitting algorithm since the measured optical signal takes a spatial average of the sample. The second challenge is the nonuniform polymer removal during NMP dissolution and O_2 PE processes, which typically initiates as the edges or cracks within the structures. This effect can also result in fitting errors since the residual polymer is not uniform within the SE measurement beam spot. Finally, this work employs MG models to calculate the residual polymer, which is only accurate when the volume fraction of the photoresist is relatively low. This is especially problematic for getting accurate estimates of the residual polymer at short etch times. However, the goal of this work is to examine processes at sufficiently long etch times so that a negligible amount of polymer remains. In this limit, the MG model allows a quantitative comparison of the NMP dissolution and O_2 PE processes, of which the former is slightly more effective.

IV. CONCLUSIONS

This research investigates the effectiveness of various resist removal techniques, including thermal desorption, NMP dissolution, O_2 PE in the fabrication of porous nanolattices. The experimental data indicate that thermal treatment at 550 °C is most effective at polymer removal, resulting in the lowest measured effective index of 1.0912 with negligible residual polymer. However, the process is long and requires more than 14 h of treatment. NMP solvent dissolution is an effective alternative, which after 15 min resulted in nanolattices with the measured index of 1.1336. Using an MG model, the corresponding residual polymer in the nanolattice can be calculated to be 7.3% by volume. In comparison to NMP, O_2 PE has a slower polymer removal rate and resulted in a higher index of 1.1536 and residual polymer of 10.7%. This research can improve the fabrication of nanolattices and can find applications in functional nanostructures, nanoarchitected materials, and nanophotonics.

ACKNOWLEDGMENTS

This work was performed at UT Austin Texas Materials Institute (TMI), the Nanomanufacturing System for Mobile Computing and Energy Technologies (NASCENT), and Texas Nanofabrication Facilities, which is supported by the National Science Foundation (NSF) as part of the National Nanotechnology Coordinated Infrastructure (NNCI) Grant No. NNCI-2025227. This work was funded by the Energy Institute at the University of Texas at Austin.

AUTHOR DECLARATIONS

Conflict of interest

The authors have no conflicts to disclose.

Author Contributions

Vijay Anirudh Premnath: Data curation (equal); Formal analysis (equal); Investigation (equal); Methodology (equal); Validation (equal); Visualization (equal); Writing – original draft (equal); Writing – review & editing (equal). **Chih-Hao Chang:** Conceptualization (equal); Data curation (equal); Formal analysis (equal); Funding acquisition (equal); Investigation (equal); Methodology (equal); Project administration (equal); Resources (equal); Supervision (equal); Validation (equal); Visualization (equal); Writing – original draft (equal); Writing – review & editing (equal).

DATA AVAILABILITY

The data that support the findings of this study are available within the article.

REFERENCES

[1]T. A. Schaedler, A. J. Jacobsen, A. Torrents, A. E. Sorensen, J. Lian, J. R. Greer, L. Valdevit, and W. B. Carter, Science **334**, 962 (2011).
[2]J. Bauer, L. R. Meza, T. A. Schaedler, R. Schwaiger, X. Zheng, and L. Valdevit, Adv. Mater. **29**, 40 (2017).
[3]L. R. Meza, S. Das, and J. R. Greer, Science **345**, 1322 (2014).
[4]X. Zheng *et al.*, Science **344**, 1373 (2014).
[5]Y. Zhao, W. Wan, Y. Chen, R. Erni, C. A. Triana, J. Li, C. K. Mavrokefalos, Y. Zhou, and G. R. Patzke, Adv. Energy Mater. **10**, 2002228 (2020).
[6]X. A. Zhang, A. Bagal, E. C. Dandley, J. Zhao, C. J. Oldham, B.-I. Wu, G. N. Parsons, and C.-H. Chang, Adv. Funct. Mater. **25**, 6644 (2015).

[7]L. C. Montemayor, L. R. Meza, and J. R. Greer, Adv. Eng. Mater. **16**, 184 (2014).
[8]R. C. Ng, R. Mandal, R. J. Anthony, and J. R. Greer, SPIE Proc. **10124**, 101241E (2017).
[9]V. Harinarayana and Y. C. Shin, Opt. Laser Technol. **142**, 107180 (2021).
[10]R. A. Borisov, G. N. Dorojkina, N. I. Koroteev, V. M. Kozenkov, S. A. Magnitskii, D. V. Malakhov, A. V. Tarasishin, and A. M. Zheltikov, Appl. Phys. B **67**, 765 (1998).
[11]L. R. Meza and J. R. Greer, J. Mater. Sci. **49**, 2496 (2014).
[12]S. K. Saha, D. Wang, V. H. Nguyen, Y. Chang, J. S. Oakdale, and S.-C. Chen, Science **366**, 105 (2019).
[13]V. Hahn, P. Kiefer, T. Frenzel, J. Qu, E. Blasco, C. B. Kowollik, and M. Wegener, Adv. Funct. Mater. **30**, 1907795 (2020).
[14]H. W. P. Koops, R. Weiel, D. P. Kern, and T. H. Baum, J. Vac. Sci. Technol. B **6**, 477 (1988).
[15]A. Botman, J. J. L. Mulders, and C. W. Hagen, Nanotechnology **20**, 372001 (2009).
[16]C. V. Shank and R. V. Schmidt, Appl. Phys. Lett. **23**, 154 (1973).
[17]J.-H. Jang, C. K. Ullal, M. Maldovan, T. Gorishnyy, S. Kooi, C. Koh, and E. L. Thomas, Adv. Funct. Mater. **17**, 3027 (2007).
[18]J. Y. Cheng, C. A. Ross, H. I. Smith, and E. L. Thomas, Adv. Mater. **18**, 2505 (2006).
[19]C. A. Ross, K. K. Berggren, J. Y. Cheng, Y. S. Jung, and J.-B. Chang, Adv. Mater. **26**, 4386 (2014).
[20]S. Jeon, J.-U. Park, R. Cirelli, S. Yang, C. E. Heitzman, P. V. Braun, P. J. A. Kenis, and J. A. Rogers, Proc. Natl. Acad. Sci. U.S.A. **101**, 12428 (2004).
[21]C.-H. Chang, L. Tian, W. R. Hesse, H. Gao, H. J. Choi, J.-G. Kim, M. Siddiqui, and G. Barbastathis, Nano Lett. **11**, 2533 (2011).
[22]X. A. Zhang, I.-T. Chen, and C.-H. Chang, Nanotechnology **30**, 352002 (2019).
[23]J. Wen, Y. Zhang, and M. Xiao, Adv. Opt. Photonics **5**, 1 (2013).
[24]I.-T. Chen, F. R. Poblete, A. Bagal, and C.-H. Chang, Proc. Natl. Acad. Sci. U. S. A. **119**, 38 (2022).
[25]S. M. George, Chem. Rev. **110**, 111 (2010).
[26]V. A. Premnath, I.-T. Chen, K.-C. Chien, and C.-H. Chang, J. Vac. Sci. Technol. B **40**, 062803 (2022).
[27]A. Bagal, "Multifunctional periodic 3D thin-Shell nanostructures," Ph.D. thesis (North Carolina State University, 2016).
[28]A. Rothen, Rev. Sci. Instrum. **16**, 26 (1945).
[29]V. A. Markel, J. Opt. Soc. Am. A **33**, 7 (2016).